atmosphere

MDPI

Article

Modeling Turbulent Fluctuations in High-Latitude Ionospheric Plasma Using Electric Field CSES-01 Observations

Simone Benella [1], Virgilio Quattrociocchi [1], Emanuele Papini [1], Mirko Stumpo [1], Tommaso Alberti [2], Maria Federica Marcucci [1], Paola De Michelis [2], Mirko Piersanti [3] and Giuseppe Consolini [1,*]

[1] INAF-Istituto di Astrofisica e Planetologia Spaziali, Via del Fosso del Cavaliere 100, 00133 Roma, Italy
[2] Istituto Nazionale di Geofisica e Vulcanologia, Via di Vigna Murata 605, 00143 Roma, Italy
[3] Dipartimento di Scienze Fisiche e Chimiche, Universitá degli Studi dell'Aquila, 67100 L'Aquila, Italy; mirko.piersanti@univaq.it
* Correspondence: giuseppe.consolini@inaf.it

Abstract: High-latitude ionospheric plasma constitutes a very complex environment, which is characterized by turbulent dynamics in the presence of different ion species. The turbulent plasma motion produces statistical features of both electromagnetic and velocity fields, which have been broadly studied over the years. In this work, we use electric field high-resolution observations provided by the China-Seismo Electromagnetic Satellite-01 in order to investigate the properties of plasma turbulence within the Earth's polar cap. We adopt a model of turbulence in which the fluctuations of the electric field are assimilated to a stochastic process evolving throughout the scales, and we show that such a process (i) satisfies the Markov condition (ii) can be modeled as a continuous diffusion process. These observations enable us to use a Fokker–Planck equation to model the changes in the statistics of turbulent fluctuations throughout the scales. In this context, we discuss the advantages and limitations of the proposed approach in modeling plasma electric field fluctuations.

Keywords: polar ionosphere; electric field turbulence; Markov processes

Citation: Benella, S.; Quattrociocchi, V.; Papini, E.; Stumpo, M.; Alberti, T.; Marcucci, M.F.; De Michelis, P.; Piersanti, M.; Consolini, G. Modeling Turbulent Fluctuations in High-Latitude Ionospheric Plasma Using Electric Field CSES-01 Observations. *Atmosphere* **2023**, *14*, 1466. https://doi.org/10.3390/atmos14091466

Academic Editors: Yuichi Otsuka and Christine Amory-Mazaudier

Received: 26 August 2023
Revised: 12 September 2023
Accepted: 18 September 2023
Published: 21 September 2023

1. Introduction

The dynamics of high-latitude ionospheric plasma are very complex and characterized by nonlinearity, chaos and turbulence. This region is indeed strongly connected to remote regions of the Earth's magnetosphere, as well as with the interplanetary environment, being affected by changes in solar wind conditions. In particular, in the auroral oval and in the polar cusp, the particle precipitation is accompanied by enhanced electromagnetic field turbulent fluctuations, mainly during magnetospheric substorms, especially in Ultra Low Frequency (ULF) and Extra Low Frequency (ELF) spectral ranges [1–4]. Power-law spectral densities, scaling properties of magnetic and electric field fluctuations, and non-Gaussian distribution functions of small-scale increments of velocity and magnetic field are some of the typical hallmarks of the occurrence of turbulence in the high-latitude ionosphere [5,6].

The study of ionospheric turbulence dates back to the late 1950s [5], and it has been widely demonstrated to be an extremely relevant phenomenon to understanding the formation of ionospheric irregularities, which are capable of affecting radio communication and global navigation and positioning systems (GNSS and GPS) [5,7–10]. In the topside F layer of the high-latitude ionosphere, where significant magnetic and electric field variations have been recorded, the range of scale where turbulence is relevant varies from a few meters up to over 1000 km [5]. Moreover, recent studies have shown that scale-invariance and intermittency are features of high-latitude magnetic and electric field fluctuations as well as plasma density variations and $\mathbf{E} \times \mathbf{B}$ drift velocity [6,11–18]. The emergence of broadband ELF electric field fluctuations and turbulent magnetic field fluctuations have been explained by a variety of physical mechanisms, such as the occurrence of strong shear flows, particle precipitation, and sporadic fast interactions between localized coherent plasma structures

(e.g., spatial irregularities, density depletion, convective structures, electron and ion holes, etc.) [19,20].

In the last twenty years, the availability of high-quality magnetic field and plasma density measurements from several rockets and space missions, such as, for instance, the ESA-Swarm mission, as well as ground-based observations, allowed researchers to better characterize the scaling and spectral features of magnetic field and plasma parameters. As a result of these recent studies, the intermittent character of the ionospheric magnetic and electric field fluctuations has been clearly demonstrated [11–13,15,17,18,21–29].

Recently, the multifractal character of the electric field fluctuations has been studied over a wide range of scales, proving that there is a different degree of multifractality of electric field fluctuations in the top-F2 ionospheric region between the polar cap trailing edge and the auroral region [17]. The observed differences were interpreted in terms of the different nature of turbulence due to the particle precipitation between the two polar regions.

The phenomenon of turbulence develops as a result of the formation of the Richardson cascade, accounting for the transfer of the energy injected at large scales towards small ones until dissipation occurs [30]. In the past Pedrizzetti and Novikov [31] and later Friedrich and Peinke [32] showed that the energy transfer among the different scales can be described as a Markov process in the inertial range. A similar scenario has been investigated in the framework of space plasma turbulence by Strumik and Macek [33,34] and by Benella et al. [35] from magnetohydrodynamic (MHD) scales to sub-ion ones. The common outcome of all the aforementioned works is that the coupling among different scales in a turbulent regime can be modeled by means of a Langevin equation [35,36].

These approaches allowed us to infer several useful facts about the nature of the coupling among the scales and the energy transfer both in fluid and MHD turbulence. In comparison to the fluid and interplanetary space plasma, the dynamics of ionospheric plasma are more complex, involving many different species, such as electrons, protons, oxygen, nitrogen, neutrals, etc. This implies that, at some scales, the resulting dynamics are a mix of fluid and kinetic processes so that the observed turbulence shows a higher degree of complexity. In this framework, the study of the ionospheric electric field fluctuations using non-traditional approaches, such as Markov analysis, may unveil some specific features of the observed turbulence. We remark that the investigation of electric field fluctuations could provide useful insights on the plasma drift motion, being the dynamics of plasma controlled by $\mathbf{E} \times \mathbf{B}$ drift.

In this work, the same approach applied to fluid turbulence by Renner et al. [37] is used to investigate the nature of the coupling of fluctuations at different scales for the electric field horizontal components as measured by the China Seismo-Electromagnetic Satellite-01 (CSES-01) in crossing the southern polar ionosphere. The specific aim of this work is to provide a model of the ionospheric turbulence within the polar cap by using high-resolution electric field data, using the electric field as a proxy for plasma drift velocity in this region where the magnetic field is essentially directed towards the Earth. The underlying assumption is that the energy transfer between different scales can be modeled as a stochastic process, and we seek evidence that the Fokker–Planck equation (FPE), resembling a rather simple drift-diffusion process, can represent a suited model also for high-latitude ionospheric turbulence.

The article is organized as follows. The electric field data sample gathered by the CSES-01 satellite during a polar cap crossing is introduced and characterized in Section 2. In order to apply the theory of Markov turbulence, we test the validity of the Markov condition on the polar cap electric field data sample in Section 3.1. The analysis of the Kramers–Moyal (KM) coefficients is presented in Section 3.2, and the outcome of the Fokker–Planck model is illustrated in Section 3.3. Finally, discussion and conclusions are drawn in Section 4.

2. Data

Data used in this work refer to the electric field measurements onboard CSES-01. The CSES-01 satellite was launched in February 2018 and is the first of a constellation of satellites devoted to monitoring seismo-electromagnetic phenomena. It flies on a Sun-synchronous

orbit at an altitude of ∼500 km; this means that it is in the topside F2 ionosphere. A large set of instruments, including an electric field detector (EFD) with a high sampling frequency (up to 5 kHz) and a Langmuir probe, equipped this satellite. Although CSES-01 is designed to monitor seismo-electromagnetic phenomena, its orbit, and the onboard instrumentation allow us to investigate the features of magnetic and electric field fluctuations in the ionospheric environment. In particular, because CSES-01 satellite is principally operative in a limited range of geographic latitudes ($| Lat | < 65°$), it is only occasionally operative during the crossing of the polar ionosphere. However, as a consequence of the North-South asymmetry of the geomagnetic field, the CSES-01 satellite is capable of exploring the southern polar ionosphere in some crossings.

In this work, we consider electric field data recorded by EFD instrument [38] with a sampling frequency of 5 kHz during a crossing of the southern polar cap region on 10 August 2018. We remark that we limit our analysis to this single passage because this is one of the southern polar ionosphere crossings in which CSES-01 is operative at the higher magnetic latitude so as to be able to collect data in the polar cap. Data have been downloaded from the CSES-01 site http://www.leos.ac.cn/#/home (accessed on 11 November 2020). According to a previous study [39], the selected time interval refers to a quasi-quiet period being the corresponding average values of AE-index and SYM-H index below 100 nT and above 0 nT, respectively. Here, these indices, although not specifically related to the southern polar cap status, are used as general proxies of the global magnetospheric-ionospheric status.

The electric field components used in this study are reported in Figure 1. As shown in this figure, the three components are rotated in the reference frame of the magnetic field, where x is the direction parallel to the vertical magnetic field, whereas y and z lie on the transverse plane.

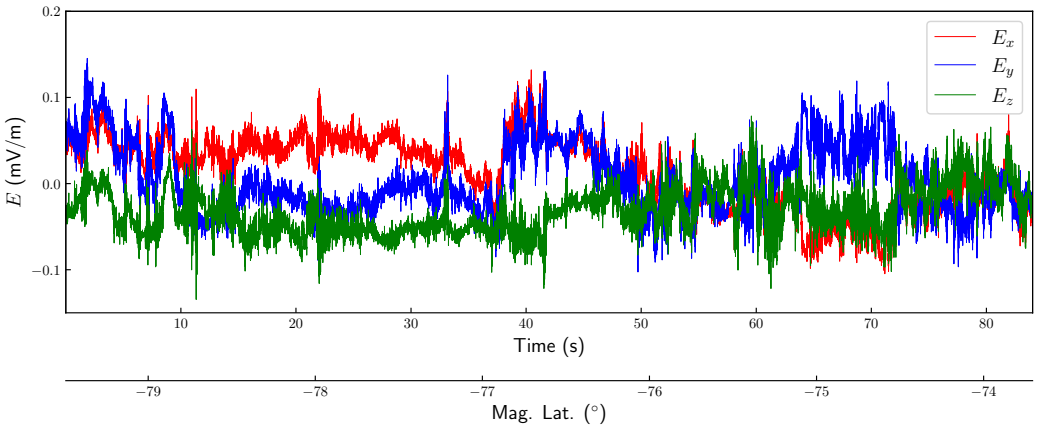

Figure 1. Electric field data of the southern polar cap crossing on 2018 August 10 gathered by EFD onboard the CSES-01 satellite.

By computing the power spectrum of the electric field components, we observe a certain degree of isotropy since the power of the three components, along vertical and transverse directions, overlap each other, Figure 2. The trend shown by the three components exhibits the typical flattening due to instrumental noise at frequencies above ∼2000 Hz. At lower frequencies, different regions can be identified. For frequencies $f \in [40, 600]$ Hz, a flattening of the electric field PSD is observed, whereas at $f \in [600, 1000]$ Hz, a cutoff is present. The PSD flattening could be a consequence of the multi-ion character of ionospheric plasma, which manifests in contiguous multiple regimes, both MHD and kinetic, due to different physical processes [28,29]. We may note that assuming an average electron density of $n_e \sim 10^5$ cm^{-3}, we obtain an inertial length $\eta_e \sim 0.017$ km which roughly corresponds to a frequency $f = v_s/\eta_e \simeq 500$ Hz where $v_s = 7.8$ km/s is the satellite velocity. This frequency is well in agreement with the end of the flattening region observed in the PSD. We remark that similar spectral features were observed by Consolini et al. [17] by

analyzing the spectral features of electric field components at the trailing edge of the polar cap, a region where the plasma motion could be characterized by strong shear flows.

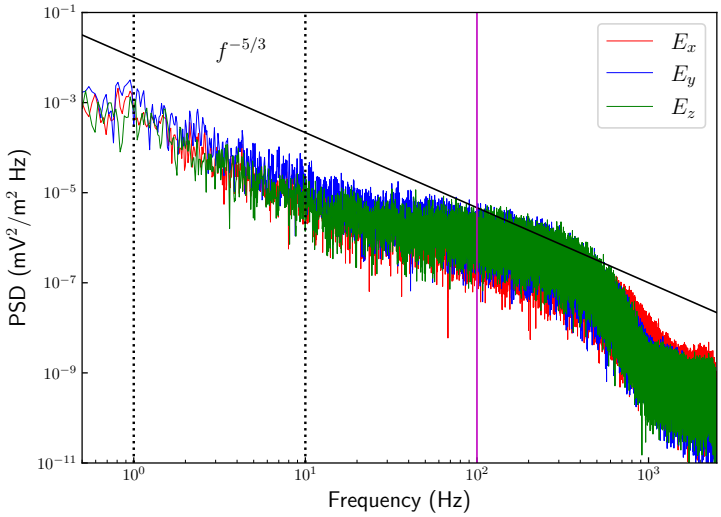

Figure 2. Power spectral density of the electric field components. Vertical dashed lines indicate the frequency interval used in the data analysis. The black solid line shows the $f^{-5/3}$ trend as a reference.

At lower frequencies, all the three power spectra have a quasi power-law trend, $PSD \simeq f^{-5/3}$ whose spectral exponents $\beta \simeq 5/3$ is consistent with that predicted by Kolmogorov K41 theory of turbulence at fluid scales, as well as, with the occurrence of electrostatic drift wave, shear-flow or density gradient turbulence [5,40], see Figure 2. Similar spectral features have been observed in the range of frequencies from 10 Hz to 100 Hz in the high-latitude ionosphere at altitudes about 430 km by the Aureol 3 satellite according to Mounir et al. [41], and from the ICI-2 sounding rocket according to Spicher et al. [11].

Another relevant feature to be noted is that the spectra in the investigated domain overlap, suggesting that the turbulence is also nearly-isotropic in this region, Mounir et al. [41]. In order to investigate the properties of turbulence of the ionospheric plasma within the polar cap, we test the Markov condition on the electric field fluctuations at fluid scales. The vertical dashed lines in Figure 2 indicate the time-scale interval considered in the following section. We limit ourselves to this short interval of frequencies/time scales because of the limited statistics available at small/longer frequencies/time scales. Assuming that there is a linear correspondence between frequencies and wavenumbers, i.e., supposing Taylor's hypothesis to be valid, $k = f/v_s$ where $v_s \simeq 7.8$ km/s is the satellite velocity, the selected time interval corresponds to the explored scales between $\sim$ 390 m and $\sim$ 3900 m. The validity of Taylor's hypothesis stands on the assumption that transit time is faster than the evolution time of the electric field at the investigated time scale. This corresponds to the assumption that the observed temporal fluctuations are principally due to Doppler-shifted and stationary spatial variations (see, e.g., [17–19,42] and references therein).

3. Analysis and Results

3.1. Testing the Markov Property

The fundamental quantity that we use in the analysis are the fluctuations of the electric field, defined as follows

$$e_i(\tau) \doteq E_i(t+\tau) - E_i(t). \tag{1}$$

The index $i = \{x, y, z\}$ denotes the three components in the magnetic field reference frame. In order to envision electric field fluctuations in the Markov process theory, we assume $e_i(\tau)$ to be a stochastic process across the time scales τ. In order to deal with Markov processes, it is then necessary to introduce the transition probabilities of the process barely mentioned. The probability of observing the electric field increment $e_{i,1}$ at the scale τ_1 given

the increments $e_{i,2}$ at the scale τ_2, under the condition $\tau_1 < \tau_2$, can be defined through the Bayes' formula as

$$p(e_{i,1}, \tau_1 | e_{i,2}, \tau_2) = \frac{p(e_{i,1}, \tau_1; e_{i,2}, \tau_2)}{p(e_{i,2}, \tau_2)}. \quad (2)$$

The function $p(e_{i,1}, \tau_1; e_{i,2}, \tau_2)$ indicates the joint probability density of the increments. The same definition can be extended to define high-order conditional probabilities. The stochastic process $e_i(\tau)$ is a Markov process if the transition probabilities fulfill the condition

$$p(e_{i,1}, \tau_1 | e_{i,2}, \tau_2; \ldots; e_{n,i}, \tau_n) = p(e_{i,1}, \tau_1 | e_{i,2}, \tau_2), \quad (3)$$

with $\tau_1 < \tau_2 < ... < \tau_n$. A natural consequence of Equation (3) is that the n-point joint probability density can be written as a product of n two-point transition probabilities, i.e.,

$$p(e_{i,1}, \tau_1; e_{i,2}, \tau_2; \ldots; e_{n,i}, \tau_n) = p(e_{i,1}, \tau_1 | e_{i,2}, \tau_2) \ldots p(e_{n-1,i}, \tau_{n-1} | e_{n,i}, \tau_n) p(e_{n,i}, \tau_n). \quad (4)$$

The two-point transition probability between the states $e_{i,1}$ and $e_{i,3}$, i.e., the probability of observing the value $e_{i,1}$ of the increment at scale τ_1 given the value $e_{i,3}$ at scale τ_3, can be rewritten by using the Markov condition (3) in the Chapman–Kolmogorov (CK) equation [43],

$$p(e_{i,1}, \tau_1 | e_{i,3}, \tau_3) = \int_{-\infty}^{+\infty} p(e_{i,1}, \tau_1 | e_{i,2}, \tau_2) p(e_{i,2}, \tau_2 | e_{i,3}, \tau_3) de_{i,2}, \quad (5)$$

where the integral is evaluated on any value $e_{i,2}$ of the increment at an intermediate scale τ_2 such that $\tau_1 < \tau_2 < \tau_3$. It is sometimes convenient to deal with joint PDFs instead of conditional ones, as in the case of small data samples or, more in general, for those processes that are not properly sampled in a given number of available data points. In this case, by applying the Bayes' Formula (2) to the CK integral (5) we obtain

$$p(e_{i,1}, \tau_1; e_{i,3}, \tau_3) = \int_{-\infty}^{+\infty} p(e_{i,1}, \tau_1 | e_{i,2}, \tau_2) p(e_{i,2}, \tau_2; e_{i,3}, \tau_3) de_{i,2}. \quad (6)$$

Since the polar cap crossing last few tens of seconds and we are interested in fairly large scales—fluid scales, i.e., up to ∼0.5 s—we used Equation (6) to perform the test. Results obtained by analyzing the y-component are shown in Figure 3 for three separations $\tau_2 - \tau_1$: 0.005 (corresponding to the magenta line in Figure 2), 0.05 and 0.5 s, (corresponding to the dashed lines appearing in Figure 2).

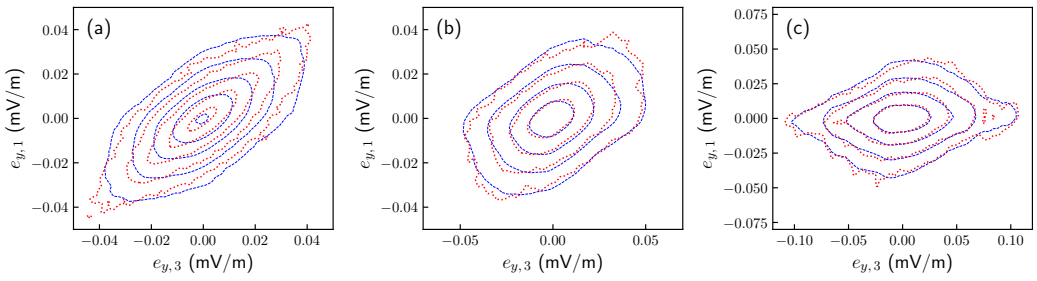

Figure 3. CK test on the fluctuations of the y-component of the electric field at three different scale separations: 0.005 (**a**), 0.05 (**b**) and 0.5 (**c**) s. The empirical joint PDF (red) is reported along with the PDF estimated through the CK relation (blue), and they are compared by superimposing PDF level curves.

By inspecting the comparison between level curves of the l.h.s. of Equation (6)—empirical PDF, reported in red—and the integral on the r.h.s.—CK PDF, reported in blue—we conclude that a remarkable deviation is observed in the case $\tau_2 - \tau_1 = 0.005$ s, whereas for fluctuations evaluated at larger time separations the contours are in agreement. These results suggest that at fluid scales the stochastic process described by electric field fluctua-

tions satisfies the Markov property whereas, when typical scales in the mixed MHD/kinetic domain are considered, the dynamics in scale may have a more complex character, e.g., the information necessary to describe the fluctuation observed at a certain scale in not fully enclosed in the scale immediately above, i.e., the Markov condition is not satisfied. Analogous results **can be** obtained also for the other components.

We conclude this section by stating that electric field fluctuations of ionospheric plasma, and in particular of the plasma drift velocity, satisfy the Markov condition at fluid scales. This property can be explained as a *memoryless* process throughout the scales, meaning that the information about a state of the system at a given scale is contained in the next higher one. The validity of the Markov condition allows us to perform the Kramers–Moyal (KM) analysis and then build a model of electric field fluctuations based on the FPE.

3.2. Kramers–Moyal Coefficient Analysis

The aim of this work is to investigate the properties of turbulence in the ionospheric plasma, focusing on the electric field components contributing to the plasma drift motion; hence, in the following section, we analyze the set of transverse electric field fluctuations $e_\perp = \{e_y, e_z\}$. The differential form of the CK equation expresses the time evolution of the transition probability, and it is called *master equation*, which can be expressed into the form of a KM expansion, i.e.,

$$-\frac{\partial}{\partial \tau} p(e_\perp, \tau | e'_\perp, \tau') = \mathcal{L}_{KM}(e_\perp, \tau) p(e_\perp, \tau | e'_\perp, \tau'). \tag{7}$$

The operator $\mathcal{L}_{KM}(e_\perp)$ is the KM operator, which is defined as

$$\mathcal{L}_{KM}(e_\perp, \tau) = \sum_{k=1}^{\infty} \left(-\frac{\partial}{\partial e_\perp} \right)^k D^{(k)}(e_\perp, \tau), \tag{8}$$

where the functions $D^{(k)}(e_\perp, \tau)$ denote the KM coefficients. Such coefficients are, in a general case, functions depending on both increment value $e_\perp$ and time scale τ and are defined as the limit $\delta \to 0$ of the conditional moments $M^{(k)}(e_\perp, \tau, \delta)$, i.e.,

$$D^{(k)}(e_\perp, \tau) = \frac{1}{k!} \lim_{\delta \to 0} M^{(k)}(e_\perp, \tau, \delta), \tag{9}$$

where

$$M^{(k)}(e_\perp, \tau, \delta) = \frac{1}{\delta} \mathbb{E}[(e_\perp(\tau - \delta) - e_\perp(\tau))^k | e_\perp(\tau)]. \tag{10}$$

The governing equation introduced in Equation (7), unlike the usual definition, presents a minus sign on the l.h.s. which accounts for the direction of the cascade, i.e., from large to small scales, according to Renner et al. [37]. The time evolution of the transition probability expressed by the KM expansion depends on an infinite number of coefficients contributing to the dynamics. According to Pawula's theorem, an important simplification holds for the class of stochastic processes of continuous diffusion. Indeed, it has been proven that for this class of stochastic processes, the fourth-order KM coefficient vanishes [43]. In other words, Pawula's theorem ensures that all the coefficients of order $k \geq 3$ vanish when $D^{(k)}(e_\perp, \tau) = 0$. In this fashion, the KM expansion reduces to the FPE, i.e.,

$$-\frac{\partial}{\partial \tau} p(e_\perp, \tau | e'_\perp, \tau') = \left[-\frac{\partial}{\partial e_\perp} D^{(1)}(e_\perp, \tau) + \frac{\partial^2}{\partial e_\perp^2} D^{(2)}(e_\perp, \tau) \right] p(e_\perp, \tau | e'_\perp, \tau'), \tag{11}$$

where the *drift* $D^{(1)}(e_\perp, \tau)$ is represented by the first-order KM coefficient and the *diffusion* $D^{(2)}(e_\perp, \tau)$ by the second-order one. It is worth reminding that the FPE that governs the

probability distribution function (PDF) of a certain stochastic process is equivalent to the Langevin equation:

$$-de_\perp = D^{(1)}(e_\perp, \tau)d\tau + \sqrt{2D^{(2)}(e_\perp, \tau)d\tau}\,\xi(\tau), \tag{12}$$

where the Itô's definition is used [43]. The term $\xi(\tau)$ denotes a delta-correlated Gaussian noise with unit variance. For the purposes of this work, we will approximate the KM coefficients as their finite-time version in the smallest value of δ^*, i.e.,

$$D^{(k)}_{\delta^*}(e_\perp, \tau) = \frac{1}{k!\delta^*} M^{(k)}(e_\perp, \tau, \delta^*). \tag{13}$$

As depicted in Figure 4 (circles), first- and second-order KM coefficients are both functions of the intensity of the fluctuation $e_\perp$ and the separation time scale τ. The dependence on the fluctuation intensity can be parameterized via linear/quadratic functions as follows

$$D^{(1)}_{\delta^*}(e_\perp, \tau) = -\gamma(\tau)e_\perp \tag{14}$$

$$D^{(2)}_{\delta^*}(e_\perp, \tau) = \alpha(\tau) + \beta(\tau)e^2_\perp. \tag{15}$$

The best fit of drift and diffusion scale-dependent parameters $\gamma(\tau)$, $\alpha(\tau)$ and $\beta(\tau)$ are indicated by solid lines of Figure 4. Concerning Pawula's theorem and the possibility of reducing the scale-to-scale process to a continuous diffusion one, the right panel of Figure 4 shows the trend of the fourth-order KM coefficient. Since it vanishes approximately over the whole interval of scales considered in our analysis, we assume Pawula's theorem to be reasonably satisfied.

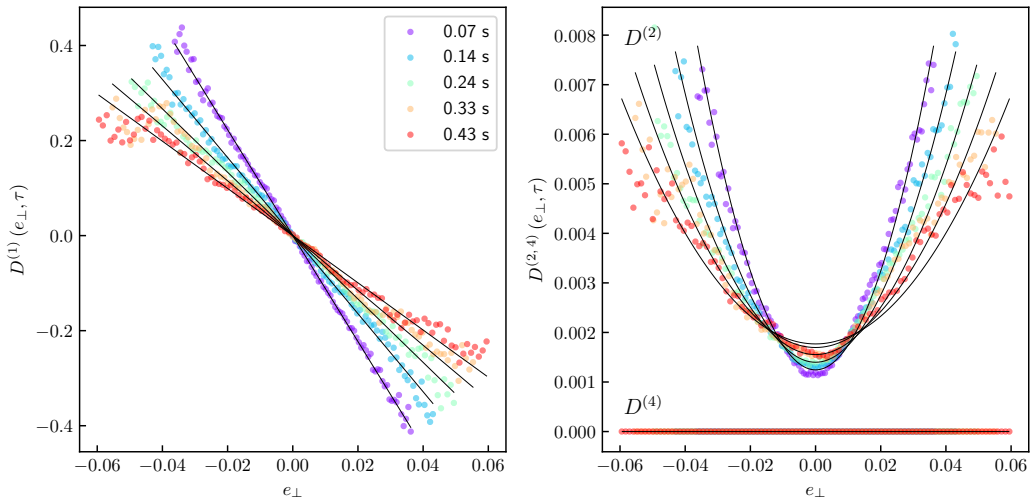

Figure 4. First-, second-, and fourth-order KM coefficients (circles) evaluated at different time scales. Black solid lines indicate the parameterizations of Equations (14) and (15).

The dependence of drift and diffusion parameters on the separation time scale τ is found to follow approximately a power-law trend

$$\{\alpha, \beta, \gamma\}(\tau) = A\tau^\mu. \tag{16}$$

The prefactors A and the exponents μ can then be fitted from electric field data, and the values obtained are listed in Table 1.

Table 1. Parameters of KM coefficients estimated from electric field fluctuations $e_\perp$ measured along the transverse direction to the mean magnetic field.

	α	β	γ
A	$[2.13 \pm 0.02] \times 10^{-3}$	0.79 ± 0.02	3.35 ± 0.03
μ	0.25 ± 0.01	-0.87 ± 0.02	-0.56 ± 0.01

3.3. Fokker–Planck Model of Electric Field Fluctuations

In the previous section, we provided a rather compact analytic expression for first- and second-order KM coefficients as a function of both fluctuation intensity and time scale. Moreover, the fourth-order coefficient vanishes, and then the master equation of the process is the FPE. In the following section, we solve numerically the FPE starting from a large-scale PDF in order to provide a consistency check of such a continuous diffusion modeling of turbulent electric field fluctuations. The numeric integration of the model is performed by using the CK Equation (5) in order to propagate the approximate solution for small steps δ. According to Risken and Caugheyz [43], the transition PDF for a continuous diffusion process with arbitrary $D^{(1)}$ and $D^{(2)}$ is the so-called Fokker–Planck propagator

$$p(e_\perp, \tau, \delta) = \frac{1}{\sqrt{2\pi D^{(2)}(e_\perp, \tau)\delta}} \exp\left\{ \frac{[e_\perp - D^{(1)}(e_\perp, \tau)\delta]^2}{2D^{(2)}(e_\perp, \tau)} \right\}. \tag{17}$$

Iterating this procedure, we can obtain the conditional PDF of the process at any scale. Finally, we compute the marginal PDF by multiplying with an initial condition $p(e_{\perp,0}, \tau_0)$ and integrating with respect to $e_{\perp,0}$. The comparison between empirical PDFs (circles) and those obtained through the numerical solution of the FPE (solid lines) is reported in Figure 5. The large-scale PDF is marked with a dashed line since it corresponds to the initial condition $p(e_{\perp,0}, \tau_0)$ and it has been obtained by parametrizing the PDF at $\tau = 0.5$ s with the Castaing distribution [44–46].

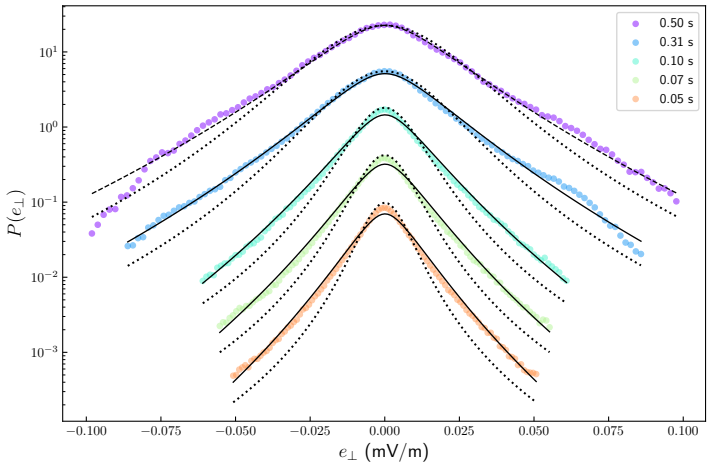

Figure 5. Comparison between the empirical PDFs (circles) and those obtained through the numerical solution of the FPE (solid lines). The dashed line marks the initial condition, whereas the dotted lines refer to the instantaneously steady-state solution of FPE.

Turbulent energy transfer constitutes a strongly out-of-equilibrium process, and since the energy is unevenly redistributed from one scale to another, thus constituting a fluctuating quantity, we expect that solutions of the Fokker–Planck model, which approximates a steady state, should fail in reproducing the observed statistics [47]. The simple form assumed for the KM coefficients, Equation (9), allows us to analytically solve the associated stationary FPE, i.e., $\partial/\partial\tau = 0$. The solution is of the form

$$p_{ST}(e_\perp, \tau) = \mathcal{N}\left[\alpha(\tau) + \beta(\tau)e_\perp^2\right]^{-\frac{\gamma(\tau)}{2\beta(\tau)}-1}, \quad (18)$$

where $\mathcal{N}$ is a normalization factor. There is still a dependence upon the time scale τ in Equation (18), which is due to the scale dependence of the drift and diffusion coefficients. This allows us to interpret the steady-state solution for a given τ as a local assumption of stationarity in the proximity of the scale τ. Predictions of this instantaneous steady-state approximation are indicated by dotted curves of Figure 5. As expected, a remarkable deviation between empirical PDFs (circles) and local, steady-state solution of FPE is found, resembling previous results obtained in the case of hydrodynamic turbulence [47].

4. Discussion and Conclusions

In this work, we presented a data-driven model of turbulent electric field fluctuations in the high-latitude ionosphere by using a polar cap crossing of the CSES-01 satellite. By inspecting the PSD, we have identified an interval at frequencies below 25 Hz where it is possible to find a spectral domain $\sim f^{-5/3}$, which corresponds to turbulent fluctuations related to the plasma motions at scales larger than 300 m. In this range of frequencies, i.e., for 2.5 Hz $\leq$ f $\leq$ 25 Hz, we have explored the Markovian character of the electric field fluctuations and our results support its validity at fluid scales, whereas a deviation between the empirical PDFs and the CK prediction is found when approaching the kinetic range. These results highlight that fluctuations of transverse electric field components, and thus, of the plasma drift velocity, constitute a proper test sample for stochastic modeling. The observed Markovian nature of the fluctuations is expected to hold for turbulent media since it has been widely tested on a great variety of data samples, ranging from fluid experiments and/or direct numerical simulations to space plasmas [33,37,48]. The reason behind this is that the Markov property in this context can be interpreted as the manifestation of a *memoryless* process throughout the scales, in which the information necessary to predict the observed state of the system at a given scale is fully contained in the next higher scale. Hence, the turbulence cascade, when envisioned as a Markovian process, loses memory about its origin (i.e., forcing), thus relating such a statistical property to the universality of turbulence. At smaller scales, the Markovian character of fluctuations breaks, suggesting that the inertial energy transfer mechanism is affected by kinetic processes associated with different ionic species and/or by the occurrence of energy dissipation.

The analysis of the KM coefficients has demonstrated how KM expansion can be truncated at the second order so that the evolution of the conditional probability reduces to the FPE. This allows us to model the electric field fluctuations through the Langevin equation. Furthermore, by solving the associated FPE, we have shown that such a model is capable of reproducing the observed time-scale evolution of the electric field fluctuation statistics. On the other hand, we observe a small deviation between empirical and predicted distributions around the core of the PDFs, especially when moving towards small scales. Such a deviation can be interpreted in terms of the accuracy in the parameterization of the KM coefficients, as we show below. In order to support this hypothesis and provide a quantitative indication of the goodness of the model, in fact, we analyze the noise term obtained by inverting the Langevin equation:

$$\xi(\tau) = \frac{e_\perp(\tau) - e_\perp(\tau+\delta) - D^{(1)}(e_\perp, \tau)\delta}{\sqrt{2D^{(2)}(e_\perp, \tau)\delta}}. \quad (19)$$

By using the analytical expression of Equations (14) and (15) for drift and diffusion terms, we calculate the noise term scale-by-scale by using electric field measurements in Equation (19). Despite the statistics of the noise results in a close to zero average value, i.e., $\langle\xi\rangle \sim 0.004$, and an approximately unit variance, i.e., $|1 - (\langle\xi^2\rangle - \langle\xi\rangle^2)| \sim 0.067$, its distribution is far from how it should be. The statistics of the noise term at different scales are shown in the

left panel of Figure 6 (circles) and are compared with the Gaussian (dashed line) distribution expected from the theory.

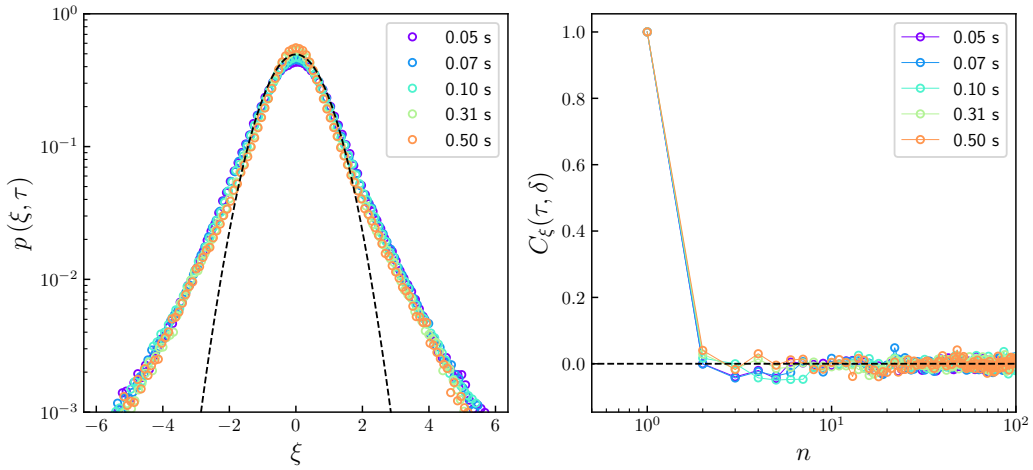

Figure 6. Left panel: PDFs of the noise at different scales. The dashed line refers to the Gaussian PDF expected from the theory. **Right panel**: the autocorrelation function of the noise term at the different timescales. The time lag n is given in units of 0.05 s.

As a second step, we investigate the autocorrelation of the noise for different time lags. In this case, Figure 6 (right panel), the autocorrelation function shows how the noise is delta-correlated in the inertial range, confirming the validity of the Markov condition previously tested by means of the CK equation. Thus, we conclude that the Fokker–Planck model proposed in this work satisfies the conditions of zero-mean, unit-variance, delta-correlated noise of the associated Langevin process, but a part of the heavy-tailed statistics of turbulent electric field fluctuations is not captured by the simple drift and diffusion parameterizations introduced here, resulting in a heavy-tail distribution of the noise term, which instead should have been Gaussian. Analogous results have been previously found in the field of hydrodynamic turbulence, highlighting the non-Gaussian nature of the random force of the turbulent fluctuations for a Langevin model of turbulent fluctuations [49,50]. In connection with this, we argue that in our case, such a Langevin model can be improved by refining the parameterization of drift and diffusion terms since by inspecting Figure 4 it is evident how the simple parametric form introduced in Equations (14) and (15) is sometimes unable to accurately describe the empirical KM coefficients, especially in the case of diffusion.

According to some previous studies (see, e.g., refs. [11,42], and references therein) a possible mechanism generating the turbulence inside the polar cap is the gradient-drift instability, which is capable of generating coherent plasma structures, generally named plasma patches. The stochastic dynamics of such coherent structures may be at the basis of the observed turbulence in the polar cusp, as suggested in some previous works [20,51,52], generating also turbulent electric field fluctuations, as clearly shown by Gondarenko and Gudzar [53,54]. These turbulent fluctuations in the electric field are generated by the nonlinear evolution of the primary gradient drift instability and are related to the horizontal motion of these structures [54]. In this framework, our results would represent a starting point to investigate via the electric field the turbulent dynamics of coherent density plasma structures in the polar cusp. Clearly, at the present stage, this is just a speculation that has to be substantiated by further studies and analysis.

In conclusion, here we have presented a different approach to investigating the statistical features of ionospheric plasma turbulence that may be put to use in order to better comprehend the role played by turbulence in producing, for instance, aberrations in the high-latitude F2 region. Further studies and analyses are necessary to better relate our model of electric field fluctuations to the dynamics of ionospheric plasma irregularities and to extend it to different ionospheric and/or geomagnetic disturbance conditions.

Author Contributions: Conceptualization, G.C. and S.B.; methodology, S.B. and G.C.; software, S.B. and M.S.; formal analysis, S.B. and V.Q.; investigation, S.B., V.Q., E.P., M.S., T.A., M.F.M., P.D.M., M.P. and G.C.; data curation, E.P. and M.P.; writing—original draft preparation, G.C., S.B. and V.Q.; writing—review and editing, S.B., V.Q., E.P., M.S., T.A., M.F.M., P.D.M., M.P. and G.C.; supervision, G.C. and S.B.; funding, G.C., M.P. and P.D.M. All authors have read and agreed to the published version of the manuscript.

Funding: This research received financial support from the Italian Space Agency under the contract ASI "LIMADOU Scienza+" No. 2020-31-HH.0.

Data Availability Statement: The original EFD data taken by CSES-01 are available at http://www.leos.ac.cn/#/home (accessed on 11 November 2020).

Acknowledgments: This work is in the framework of the CSES-LIMADOU Collaboration (http://cses.roma2.infn.it). V. Quattrociocchi thanks the Italian Space Agency for the financial support under the contracts ASI "LIMADOU Scienza+" No. 2020-31-HH.0 and ASI "LIMADOU-2 fase B2/C/D/E1".

Conflicts of Interest: The authors declare no conflict of interest.

Abbreviations

The following abbreviations are used in this manuscript:

AE	Auroral Electrojet
CK	Chapman–Kolmogorov
CSES	China-Seismo-Electromagnetic Satellite
EFD	Electric Field Detector
ELF	Extra Low Frequency
FPE	Fokker–Planck Equation
GNNS	Global Navigation Satellite System
GPS	Global Positioning System
KM	Kramers Moyal
MHD	Magnetohydrodynamics
PDF	Probability Distribution Function
PSD	Power Spectral Density
ULF	Ultra Low Frequency

References

1. Earle, G.D.; Kelley, M.C.; Ganguli, G. Large velocity shears and associated electrostatic waves and turbulence in the auroral F region. *J. Geophys. Res. Space Phys.* **1989**, *94*, 15321–15333. [CrossRef]
2. Lagoutte, D.; Cerisier, J.C.; Plagnaud, J.L.; Villain, J.P.; Forget, B. High-latitude ionospheric electrostatic turbulence studied by means of the wavelet transform. *J. Atmos. Terr. Phys.* **1992**, *54*, 1283–1293. [CrossRef]
3. Kintner, P.M.; Franz, J.; Schuck, P.; Klatt, E. Interferometric coherency determination of wavelength or what are broadband ELF waves? *J. Geophys. Res.* **2000**, *105*, 21237–21250. [CrossRef]
4. Hysell, D.; Shume, E. Electrostatic plasma turbulence in the topside equatorial F region ionosphere. *J. Geophys. Res. Space Phys.* **2002**, *107*, SIA-1–SIA-12. [CrossRef]
5. Kintner, P.M.; Seyler, C.E. The status of observations and theory of high latitude ionospheric and magnetospheric plasma turbulence. *Space Sci. Rev.* **1985**, *41*, 1572–9672. [CrossRef]
6. Golovchanskaya, I.V.; Ostapenko, A.A.; Kozelov, B.V. Relationship between the high-latitude electric and magnetic turbulence and the Birkeland field-aligned currents. *J. Geophys. Res. (Space Phys.)* **2006**, *111*, A12301. [CrossRef]
7. Booker, H.G. Turbulence in the Ionosphere with Applications to Meteor-Trails Radio-Star Scintillation, Auroral Radar Echoes, and Other Phenomena. *J. Geophys. Res.* **1956**, *61*, 673–705. [CrossRef]
8. Booker, H.G. A theory of scattering by nonisotropic irregularities with application to radar reflections from the aurora. *J. Atmos. Terr. Phys.* **1956**, *8*, 204–221. [CrossRef]
9. Dagg, M. The origin of the ionospheric irregularities responsible for radio-star scintillations and spread-F—I. Review of existing theories. *J. Atmos. Terr. Phys.* **1957**, *11*, 133–138. [CrossRef]
10. Dagg, M. The origin of the ionospheric irregularities responsible for radio-star scintillations and spread-F—II. Turbulent motion in the dynamo region. *J. Atmos. Terr. Phys.* **1957**, *11*, 139–150. [CrossRef]
11. Spicher, A.; Miloch, W.J.; Clausen, L.B.N.; Moen, J.I. Plasma turbulence and coherent structures in the polar cap observed by the ICI-2 sounding rocket. *J. Geophys. Res. Space Phys.* **2015**, *120*, 10,959–10.978. [CrossRef]

12. Tam, S.W.Y.; Chang, T.; Kintner, P.M.; Klatt, E. Intermittency analyses on the SIERRA measurements of the electric field fluctuations in the auroral zone. *Geophys. Res. Lett.* **2005**, *32*, L05109. [CrossRef]
13. De Michelis, P.; Consolini, G.; Tozzi, R. Magnetic field fluctuation features at Swarm's altitude: A fractal approach. *Geophys. Res. Lett.* **2015**, *42*, 3100–3105. [CrossRef]
14. De Michelis, P.; Consolini, G.; Tozzi, R.; Marcucci, M.F. Scaling Features of High-Latitude Geomagnetic Field Fluctuations at Swarm Altitude: Impact of IMF Orientation. *J. Geophys. Res. (Space Phys.)* **2017**, *122*, 10,548–10.562. [CrossRef]
15. Consolini, G.; De Michelis, P.; Alberti, T.; Giannattasio, F.; Coco, I.; Tozzi, R.; Chang, T.T.S. On the Multifractal Features of Low-Frequency Magnetic Field Fluctuations in the Field-Aligned Current Ionospheric Polar Regions: Swarm Observations. *J. Geophys. Res. (Space Phys.)* **2020**, *125*, e27429. [CrossRef]
16. Consolini, G.; De Michelis, P.; Alberti, T.; Coco, I.; Giannattasio, F.; Tozzi, R.; Carbone, V. Intermittency and Passive Scalar Nature of Electron Density Fluctuations in the High-Latitude Ionosphere at Swarm Altitude. *Geophys. Res. Lett.* **2020**, *47*, e89628. [CrossRef]
17. Consolini, G.; Quattrociocchi, V.; D'Angelo, G.; Alberti, T.; Piersanti, M.; Marcucci, M.F.; De Michelis, P. Electric Field Multifractal Features in the High-Latitude Ionosphere: CSES-01 Observations. *Atmosphere* **2021**, *12*, 646. [CrossRef]
18. Consolini, G.; Quattrociocchi, V.; Benella, S.; De Michelis, P.; Alberti, T.; Piersanti, M.; Marcucci, M.F. On Turbulent Features of E × B Plasma Motion in the Auroral Topside Ionosphere: Some Results from CSES-01 Satellite. *Remote Sens.* **2022**, *14*, 1936. [CrossRef]
19. Chang, T. Colloid-like Behavior and Topological Phase Transitions in Space Plasmas: Intermittent Low Frequency Turbulence in the Auroral Zone. *Phys. Scr. Vol. T* **2001**, *89*, 80–83. [CrossRef]
20. Chang, T.; Tam, S.W.Y.; Wu, C.C. Complexity induced anisotropic bimodal intermittent turbulence in space plasmas. *Phys. Plasmas* **2004**, *11*, 1287–1299. [CrossRef]
21. Abel, G.A.; Freeman, M.P.; Chisham, G. Spatial structure of ionospheric convection velocities in regions of open and closed magnetic field topology. *Geophys. Res. Lett.* **2006**, *33*, L24103. [CrossRef]
22. Kozelov, B.V.; Golovchanskaya, I.V. Scaling of electric field fluctuations associated with the aurora during northward IMF. *Geophys. Res. Lett.* **2006**, *33*, L20109. [CrossRef]
23. Abel, G.A.; Freeman, M.P.; Chisham, G.; Watkins, N.W. Investigating turbulent structure of ionospheric plasma velocity using the Halley SuperDARN radar. *Nonlinear Process. Geophys.* **2007**, *14*, 799–809. [CrossRef]
24. Kozelov, B.V.; Golovchanskaya, I.V.; Ostapenko, A.A.; Fedorenko, Y.V. Wavelet analysis of high-latitude electric and magnetic fluctuations observed by the Dynamic Explorer 2 satellite. *J. Geophys. Res. (Space Phys.)* **2008**, *113*, A03308. [CrossRef]
25. Kozelov, B.V.; Golovchanskaya, I.V. Derivation of aurora scaling parameters from ground-based imaging observations: Numerical tests. *J. Geophys. Res. (Space Phys.)* **2010**, *115*, A02204. [CrossRef]
26. Golovchanskaya, I.V.; Kozelov, B.V. On the origin of electric turbulence in the polar cap ionosphere. *J. Geophys. Res. (Space Phys.)* **2010**, *115*, A09321. [CrossRef]
27. Golovchanskaya, I.V.; Kozelov, B.V. Properties of electric turbulence in the polar cap ionosphere. *Geomagn. Aeron.* **2010**, *50*, 576–587. [CrossRef]
28. Tam, S.W.Y.; Chang, T.; Kintner, P.M.; Klatt, E.M. Rank-ordered multifractal analysis for intermittent fluctuations with global crossover behavior. *Phys. Rev. E* **2010**, *81*, 036414. [CrossRef]
29. Tam, S.W.Y.; Chang, T. Double rank-ordering technique of ROMA (Rank-Ordered Multifractal Analysis) for multifractal fluctuations featuring multiple regimes of scales. *Nonlinear Process. Geophys.* **2011**, *18*, 405–414. [CrossRef]
30. Frisch, U. *Turbulence*; Cambridge University Press: Cambridge, UK, 1995.
31. Pedrizzetti, G.; Novikov, E.A. On Markov modelling of turbulence. *J. Fluid Mech.* **1994**, *280*, 69–93. [CrossRef]
32. Friedrich, R.; Peinke, J. Description of a turbulent cascade by a Fokker-Planck equation. *Phys. Rev. Lett.* **1997**, *78*, 863. [CrossRef]
33. Strumik, M.; Macek, W.M. Testing for Markovian character and modeling of intermittency in solar wind turbulence. *Phys. Rev. E* **2008**, *78*, 026414. [CrossRef] [PubMed]
34. Strumik, M.; Macek, W. Statistical analysis of transfer of fluctuations in solar wind turbulence. *Nonlinear Process. Geophys.* **2008**, *15*, 607–613. [CrossRef]
35. Benella, S.; Stumpo, M.; Consolini, G.; Alberti, T.; Carbone, V.; Laurenza, M. Markovian Features of the Solar Wind at Subproton Scales. *Astrophys. J. Lett.* **2022**, *928*, L21. [CrossRef]
36. Benella, S.; Stumpo, M.; Consolini, G.; Alberti, T.; Laurenza, M.; Yordanova, E. Kramers–Moyal analysis of interplanetary magnetic field fluctuations at sub-ion scales. *Rend. Lincei. Sci. Fis. E Nat.* **2022**, *33*, 721–728. [CrossRef]
37. Renner, C.; Peinke, J.; Friedrich, R. Experimental indications for Markov properties of small-scale turbulence. *J. Fluid Mech.* **2001**, *433*, 383. [CrossRef]
38. Huang, J.; Lei, J.; Li, S.; Zeren, Z.; Li, C.; Zhu, X.; Yu, W. The Electric Field Detector (EFD) onboard the ZH-1 satellite and first observational results. *Earth Planet. Phys.* **2018**, *2*, 469–478. [CrossRef]
39. Papini, E.; Piersanti, M.; D'Angelo, G.; Cicone, A.; Bertello, I.; Parmentier, A.; Diego, P.; Ubertini, P.; Consolini, G.; Zhima, Z. Detecting the Auroral Oval through CSES-01 Electric Field Measurements in the Ionosphere. *Remote Sens.* **2023**, *15*, 1568. [CrossRef]
40. Pécseli, H. Spectral properties of electrostatic drift wave turbulence in the laboratory and the ionosphere. In *Annales Geophysicae*; Copernicus GmbH: Göttingen, Germany, 2015; Volume 33, pp. 875–900.

41. Mounir, H.; Berthelier, A.; Cerisier, J.C.; Lagoutte, D.; Beghin, C. The small-scale turbulent structure of the high latitude ionosphere-Arcad-Aureol-3 observations. *Ann. Geophys.* **1991**, *9*, 725–737.
42. Basu, S.; MacKenzie, E.; Basu, S.; Coley, W.R.; Sharber, J.R.; Hoegy, W.R. Plasma structuring by the gradient drift instability at high latitudes and comparison with velocity shear driven processes. *J. Geophys. Res.* **1990**, *95*, 7799–7818. [CrossRef]
43. Risken, H.; Caugheyz, T.K. The Fokker-Planck Equation: Methods of Solution and Application, 2nd ed. *J. Appl. Mech.* **1991**, *58*, 860. [CrossRef]
44. Castaing, B.; Gagne, Y.; Hopfinger, E.J. Velocity probability density functions of high Reynolds number turbulence. *Phys. D Nonlinear Phenom.* **1990**, *46*, 177–200. [CrossRef]
45. Sorriso-Valvo, L.; Carbone, V.; Veltri, P.; Consolini, G.; Bruno, R. Intermittency in the solar wind turbulence through probability distribution functions of fluctuations. *Geophys. Res. Lett.* **1999**, *26*, 1801–1804. [CrossRef]
46. Sorriso-Valvo, L.; Marino, R.; Lijoi, L.; Perri, S.; Carbone, V. Self-consistent Castaing Distribution of Solar Wind Turbulent Fluctuations. *Astrophys. J.* **2015**, *807*, 86. [CrossRef]
47. Nickelsen, D.; Engel, A. Probing small-scale intermittency with a fluctuation theorem. *Phys. Rev. Lett.* **2013**, *110*, 214501. [CrossRef]
48. Fuchs, A.; Obligado, M.; Bourgoin, M.; Gibert, M.; Mininni, P.D.; Peinke, J. Markov property of Lagrangian turbulence. *EPL (Europhys. Lett.)* **2022**, *137*, 53001. [CrossRef]
49. Marcq, P.; Naert, A. A Langevin equation for the energy cascade in fully developed turbulence. *Phys. D Nonlinear Phenom.* **1998**, *124*, 368–381. [CrossRef]
50. Marcq, P.; Naert, A. A Langevin equation for turbulent velocity increments. *Phys. Fluids* **2001**, *13*, 2590–2595. [CrossRef]
51. Chang, T.; Tam, S.W.; Wu, C.C. Complexity in space plasmas—A brief review. *Space Sci. Rev.* **2006**, *122*, 281–291. [CrossRef]
52. Yordanova, E.; Bergman, J.; Consolini, G.; Kretzschmar, M.; Materassi, M.; Popielawska, B.; Roca-Sogorb, M.; Stasiewicz, K.; Wernik, A. Anisotropic scaling features and complexity in magnetospheric-cusp: A case study. *Nonlinear Process. Geophys.* **2005**, *12*, 817–825. [CrossRef]
53. Gondarenko, N.; Guzdar, P. Density and electric field fluctuations associated with the gradient drift instability in the high-latitude ionosphere. *Geophys. Res. Lett.* **2004**, *31*, L11802. [CrossRef]
54. Gondarenko, N.; Guzdar, P. Plasma patch structuring by the nonlinear evolution of the gradient drift instability in the high-latitude ionosphere. *J. Geophys. Res. Space Phys.* **2004**, *109*, A09301. [CrossRef]